



# Effects of H<sub>2</sub>S and H<sub>2</sub>O on carbon deposition over La<sub>0.4</sub>Sr<sub>0.5</sub>Ba<sub>0.1</sub>TiO<sub>3</sub>/YSZ perovskite anodes in methane fueled SOFCs

Shao-Hua Cui<sup>a,b</sup>, Jian-Hui Li<sup>b,c</sup>, Abhimanyu Jayakumar<sup>d</sup>, Jing-Li Luo<sup>b,\*</sup>, Karl T. Chuang<sup>b</sup>, Josephine M. Hill<sup>d</sup>, Li-Jie Qiao<sup>a,\*</sup>

<sup>a</sup> Corrosion and Protection Center, Key Laboratory for Environmental Fracture (MOE), University of Science and Technology Beijing, Beijing 100083, China

<sup>b</sup> Department of Chemical and Materials Engineering, University of Alberta, Edmonton, Alberta, Canada T6G 2G6

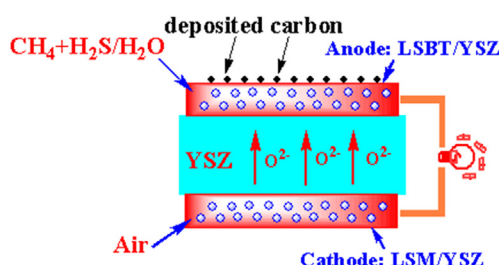
<sup>c</sup> National Engineering Laboratory for Green Chemical Productions of Alcohols–Ethers–Esters, College of Chemistry and Chemical Engineering, Xiamen University, Xiamen 361005, China

<sup>d</sup> Department of Chemical and Petroleum Engineering, University of Calgary, Calgary, Alberta, Canada T2N 1N4

## HIGHLIGHTS

- Carbon deposition became more severe with increasing exposure time and temperature.
- Carbon deposition became less severe in the presence of a current or steam.
- Introduction of H<sub>2</sub>S aggravated carbon deposition.
- Deposits could not be allayed effectively by adding H<sub>2</sub>O in the presence of H<sub>2</sub>S.

## GRAPHICAL ABSTRACT



## ARTICLE INFO

### Article history:

Received 29 August 2013

Received in revised form

19 October 2013

Accepted 26 October 2013

Available online 13 November 2013

### Keywords:

Solid oxide fuel cell

LSBT

Carbon

Hydrogen sulfide

Steam

## ABSTRACT

The effects of H<sub>2</sub>S and H<sub>2</sub>O in the methane feed on carbon deposition in a La<sub>0.4</sub>Sr<sub>0.5</sub>Ba<sub>0.1</sub>TiO<sub>3</sub> (LSBT) anode-based solid oxide fuel cell were investigated in this work under different operating conditions. Characterization was done using a combination of electrochemical, Fourier transform infra-red spectroscopy (FTIR), temperature-programmed oxidation (TPO) and X-ray photoelectron spectroscopy (XPS) measurements. As expected, carbon accumulation became more severe with increasing exposure time and operating temperature, but less severe in the presence of a current and/or steam. Addition of 0.5% H<sub>2</sub>S to the feed increased carbon accumulation and this carbon could not be removed effectively by co-feeding a small amount of steam to the anode. The resulting carbon was, however, easier to remove with oxygen as compared to that deposited by the H<sub>2</sub>S-containing dry feed.

© 2013 Elsevier B.V. All rights reserved.

## 1. Introduction

Solid oxide fuel cells (SOFCs) as energy conversion systems have received extensive attention in recent years due to their process simplicity and potential for decreased environmental impact.

\* Corresponding authors.

E-mail addresses: [jingli.luo@ualberta.ca](mailto:jingli.luo@ualberta.ca) (J.-L. Luo), [lqiao@ustb.edu.cn](mailto:lqiao@ustb.edu.cn) (L.-J. Qiao).

SOFC anode catalyst of Ni/YSZ either to form a sulfide or poison the catalyst surface [3]. Our previous studies, however, have demonstrated that H<sub>2</sub>S could strongly promote methane oxidation over sulfur resistant oxide catalysts [4].

Much work has been done to design alternative anodes that can endure the harsh environment in a SOFC. Perovskite structured materials are potential Ni-free anode candidates due to their high chemical stability and resistance to carbon accumulation and sulfur poisoning [5]. Among the variety of perovskite materials, lanthanum strontium titanate (La<sub>x</sub>Sr<sub>1-x</sub>TiO<sub>3</sub>, LST) has sufficient thermal and chemical stability under reducing conditions in the presence of H<sub>2</sub>S but relatively low catalytic activity for the fuel oxidation reaction [6]. The activity of LST, as well as the ionic conductivity, can be increased significantly by partly substituting Ba for Sr, as in La<sub>0.4</sub>Sr<sub>0.5</sub>Ba<sub>0.1</sub>TiO<sub>3</sub> (LSBT) [7].

Another limitation in the utilization of natural gas is carbon accumulation on the anode surfaces, which blocks active sites, degrades the anode microstructure and in extreme cases, destroys the integrated cell structure [8]. Carbon is produced by the catalytic decomposition of methane at the high operating temperatures of 1073–1273 K, and from CO disproportionation (the Boudouard reaction) [9]. Temperature-programmed oxidation (TPO) is often used to analyze the quantity and type of carbon accumulated on the anodes after exposure to methane (or other carbon-containing fuels). Although the TPO profile is not a fingerprint like X-ray diffraction (XRD) or Fourier transform infra-red spectroscopy (FTIR), and the peak positions are affected by the heating rate, flow rate, and amount of sample, some information on the type of carbon can be obtained from a TPO profile. Carbon oxidized at lower temperatures is more reactive and often is amorphous carbon, whereas carbon removed at higher temperatures is less reactive and often associated with graphitic carbon [10].

Although a high H<sub>2</sub>O/CH<sub>4</sub> ratio in the feed is beneficial for the suppression of carbon formation, the steam reforming of methane is an endothermic reaction that can create large temperature gradients in the anode [11,12]. Furthermore, adding too much steam to the anode chamber leads to a large decrease in the fuel cell open-circuit potential, thereby decreasing the fuel cell performance [12].

In this study, we have examined cell performance and carbon accumulation on LSBT/YSZ anodes under various operating conditions with FTIR, TPO, X-ray photoelectron spectroscopy (XPS) and electrochemical measurements. In particular, the interactions between three of the compounds of natural gas, namely CH<sub>4</sub>, H<sub>2</sub>S and H<sub>2</sub>O have been examined at 1073 K and 1123 K.

## 2. Experimental

### 2.1. Fuel cell fabrication and testing

Fuel cells were fabricated using commercial YSZ disks (fuel cell materials) as electrolytes, 300 μm in thickness and 25 mm in diameter. The porous YSZ layer was prepared using a mixture of YSZ powder (Tosoh) with 40 wt% polymethyl methacrylate (PMMA, Microbeads, Skedsmokorset, Norway) as the pore former. The mixture was powdered in a planetary ball mill, and then a paste was formed by mixing the powders with a 2:1 α-terpineol (Alfa Aesar):isopropanol solution containing 5 wt% poly vinyl butyral-co-vinyl alcohol-co-vinyl acetate (PVB, MW = 70,000–100,000, Aldrich) and 5 wt% ethyl cellulose (Aldrich). The paste was then screen printed onto one side of the YSZ electrolyte, and sintered at 1473 K for 3 h to generate a porous layer with a porosity of approximately 55 vol.%.

The LSBT precursor solution was prepared by dissolving stoichiometric amounts of lanthanum nitrate hexahydrate (La(N-O<sub>3</sub>)<sub>3</sub>·6H<sub>2</sub>O, Alfa Aesar, 99.9%), strontium nitrate (Sr(NO<sub>3</sub>)<sub>2</sub>, Sigma

Aldrich) and barium nitrate (Ba(NO<sub>3</sub>)<sub>2</sub>, Alfa Aesar 99.9%) into an aqueous solution of titanium isopropoxide (TIP, Sigma Aldrich). The TIP was stabilized in triethanolamine (TEA, Sigma Aldrich, molar ratio TIP/TEA = 1:4) to prevent hydrolysis. The total cation concentration of the solution was 1 × 10<sup>-3</sup> mol g<sup>-1</sup>. Detailed descriptions have been reported elsewhere [13].

The sintered porous anode layers were impregnated with the LSBT precursor solution in vacuum and calcined at 1073 K for 1 h in air following each impregnation step to ensure good distribution of the catalyst phase. The LSBT solution was impregnated 6 times (~12.6 wt%) to form the LSBT/YSZ composite anode.

The cathode was prepared by mixing a 1:1 mass ratio of commercial strontium doped lanthanum manganite (LSM, Nextech Materials, 5.734 m<sup>2</sup> g<sup>-1</sup>) and YSZ powders with the pore former polymethyl methacrylate (PMMA). The cathode ink was prepared using the same method as the anode paste and was applied using screen printing to form a membrane electrode assembly (MEA) with a circular effective area of 1 cm<sup>2</sup>, and then calcined in air to 1473 K for 1 h. After the MEA was sintered, 1 cm<sup>2</sup> gold and platinum pastes were painted onto the sides of the anode and cathode, respectively, which were then sintered to form the current collectors. There was an annular blank area between the electrode zone and the edge of the electrolyte disk.

The MEA was placed between two coaxial alumina tubes (inlet and outlet) to form the anode and cathode compartments. Gold current collector wires with spiral wound ends passed through the length of the inner tube (inlet). Fuel cell tests were conducted using a four-electrode setup. Glass sealant (Ceramabond, Aremco Products) was applied to seal the outer tube (outlet) directly to the outer edge of the anode side of the electrolyte. The cell was then heated in a Thermolyne F79300 tubular furnace. Before all single cell tests, the anodes were reduced in-situ at 1173 K. The cathode side of each MEA was not sealed within a tube, and its compartment was supplied with air flow of 75 mL min<sup>-1</sup>. Pure hydrogen (H<sub>2</sub>, Praxair), pure methane (CH<sub>4</sub>, Praxair), methane with 0.5% hydrogen sulfide (0.5% H<sub>2</sub>S-CH<sub>4</sub>, Praxair) and these fuels with different concentrations of water were fed at a rate of 75 mL min<sup>-1</sup> to the anode. The system was stabilized after each change of temperature and feed, before recording measurements.

Fuel cell testing was performed with standard DC and AC electrochemical techniques using a Solartron instrument (SI1287 EI). The electrochemical impedance was analyzed from 1 MHz to 0.1 Hz at open circuit voltage (OCV), with 10 mV AC amplitude.

### 2.2. Characterization of cells

A RIGAKU RU-200B Rotating anode X-ray diffraction (XRD) system with a Cu target was used to analyze phase composition of all synthesized powders under a scan rate of 2° min<sup>-1</sup>. The commercial software Jade<sup>®</sup> 5.0 was used to identify the phase structure.

Fourier transform infra-red spectroscopy (FTIR) was performed using a Nicolet 8700 (Thermo) FTIR spectrometer at room temperature. The samples were dried and mixed with KBr powders. Reference spectra with only KBr powders were acquired before each measurement and used to calculate the absorption spectra of the tested samples.

X-ray photoelectron spectroscopy (XPS) was performed using a Kratos Analytical AXIS 165. A monochromatic Al Kα source (hν = 1486.6 eV) was used at a power of 210 W, with a base pressure of 3 × 10<sup>-8</sup> Pa in the analytical chamber. Spectra were referenced to the C 1s binding energy of 284.4 eV, and were fitted using Gaussian–Lorentzian peak shapes and Shirley baselines.

The temperature-programmed oxidation (TPO) method was used to characterize and quantify the carbon deposition on the anode materials after various treatments. The samples were cooled

down to room temperature in flowing 10% H<sub>2</sub>–N<sub>2</sub>, then put in an alumina tube and loaded into the TPO apparatus and exposed to a flow of 10% O<sub>2</sub> balance He at 50 ml min<sup>−1</sup> for 1 h. The temperature was then increased from room temperature to 1173 K at 10 K min<sup>−1</sup> and the outlet gases were analyzed with the mass spectrometer (Cirrus, MKS Spectra products). Signals for  $m/z = 44$  (CO<sub>2</sub>),  $m/z = 28$  (CO only, residual N<sub>2</sub> contribution and CO<sub>2</sub> contribution to 28 removed for analysis),  $m/z = 32$  (O<sub>2</sub>),  $m/z = 18$  (H<sub>2</sub>O),  $m/z = 76$  (CS<sub>2</sub>),  $m/z = 60$  (COS),  $m/z = 64$  (SO<sub>2</sub>) and  $m/z = 48$  (SO) were monitored during the TPO experiment. Prior to the TPO analysis, the mass spectrometer signals were calibrated using gas mixtures of known concentrations.

### 3. Results and discussion

#### 3.1. Effect of exposure time

Fig. 1 shows the typical XRD patterns of the porous YSZ structure sintered at 1473 K for 3 h (Fig. 1a) and the porous YSZ impregnated with the LSBT precursor calcined at 1073 K for 1 h (Fig. 1b). LSBT with the cubic perovskite phase of SrTiO<sub>3</sub> was formed after impregnation and calcination.

To evaluate the effect of exposure time on the nature and amount of carbon accumulated, ex-situ tests were performed by exposing LSBT powder samples to methane for 10 h and 24 h under OCV conditions at 1123 K. Methane does not decompose in the gas phase at this temperature [14] but will decompose on the anode surface as follows:



$$\Delta G_{1123\text{ K}}^\circ = -32.6 \text{ kJ mol}^{-1}$$

Indeed, in these experiments with LSBT powders, carbon formation was detected by TPO as shown in Table 1 and Fig. 2.

The amount of deposited carbon can be determined by integrating the area under the TPO curves in Fig. 2 and normalizing by

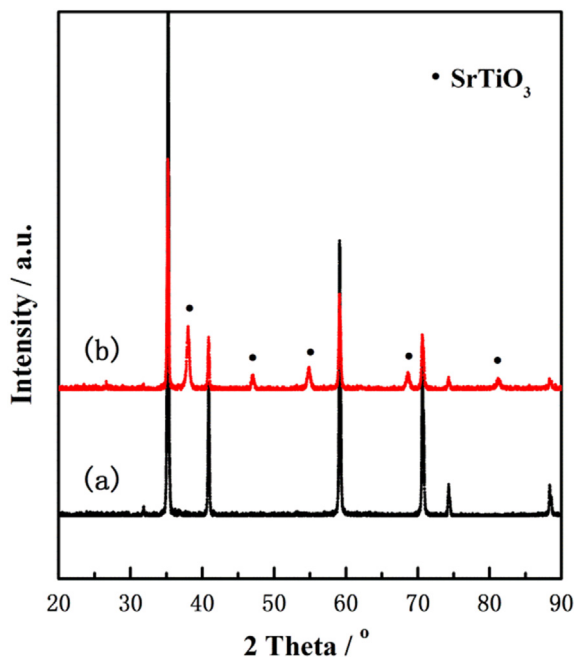


Fig. 1. XRD patterns of (a) YSZ structure sintered at 1473 K for 3 h and (b) porous YSZ impregnated with the LSBT precursor calcined at 1073 K for 1 h.

Table 1

Amount of CO<sub>2</sub>, CO and H<sub>2</sub>O produced during TPO tests of LSBT powders exposed to CH<sub>4</sub> at 1123 K.

Sample	Time	Sample mass (g)	CO <sub>2</sub> (mol)	CO (mol)	H <sub>2</sub> O (mol)	Total carbon (mol C g <sup>−1</sup> )
LSBT	10 h	0.1680	7.83E-4	5.99E-5	3.98E-5	0.5E-2
LSBT	24 h	0.1680	2.03E-3	1.9E-4	7.74E-5	1.32E-2

the mass of LSBT in each sample [15]. The amount of carbon increased from 0.5E-2 to 1.32E-2 mol g<sup>−1</sup> as the exposure time increased from 10 to 24 h. The temperature at which the carbon was oxidized during the TPO tests also increased. After exposure to CH<sub>4</sub> for 10 h, the TPO peaks for CO<sub>2</sub> evolution ranged from 500 K to 940 K, but the upper limit increased to 1000 K after the longer (i.e., 24 h) exposure time, suggesting that the stability of the carbon deposits increased with exposure time.

Generally, methane dissociation leads to the formation of a range of products from more easily oxidizable CH<sub>x</sub> ( $x = 1-3$ ) fragments to less reactive carbon which eventually orders itself into graphite-like layers [16]. There were two CO<sub>2</sub> peaks for the LSBT powders exposed to methane for both exposure times, shown in the inset of Fig. 2a, suggesting that two different types of carbon were formed. The lower temperature peak was significantly smaller and could be from CH<sub>x</sub>,  $x = 1-3$ , fragments, whereas, the higher temperature peak could be graphite or graphite-like carbon. The magnitudes of the higher temperature CO<sub>2</sub> peaks were ~100 times those of the lower temperature CO<sub>2</sub> peaks for both samples.

Similarly there were two main H<sub>2</sub>O peaks observed for both samples (Fig. 2b), and these peaks corresponded to the temperatures of the CO<sub>2</sub> peaks. The magnitudes of the H<sub>2</sub>O peaks were similar to the magnitudes of the low temperature CO<sub>2</sub> peaks but approximately two orders of magnitude smaller than the high temperature CO<sub>2</sub> peaks, (Fig. 2c), which is consistent with the assignment of the low temperature peaks to CH<sub>x</sub> species and the higher temperature peaks to C only.

The presence of CH<sub>x</sub> fragments was confirmed by FTIR analysis (Fig. 3). A broad absorption band near 3000 cm<sup>−1</sup> was observed, which is related to C–H bonds (2853–2962 cm<sup>−1</sup>), assigned to CH, CH<sub>2</sub> and CH<sub>3</sub> [17,18]. Based on Fig. 2c, the amount of CO<sub>2</sub> and H<sub>2</sub>O formed at low temperatures are in the same order of magnitude. The estimated C:H ratios, found by integrating the areas of the corresponding peaks formed in lower temperature, were approximately 2.0 and 1.3 for the LSBT powders exposed to CH<sub>4</sub> for 10 h and 24 h, respectively.

XPS analysis was used to identify the near-surface composition of the powders after exposure to CH<sub>4</sub> at 1123 K for different periods of time. Fig. 4 shows the XPS analysis of the binding energy of carbon on the anode surface compared with that for a fresh sample. The XPS spectra of both samples had asymmetric peaks centered at 284.5 eV with an extended tail at the higher energy region. This asymmetric peak is consistent with sp<sup>2</sup> hybridized graphite-like carbon [19]. The carbon accumulated on the sample treated in CH<sub>4</sub> for 24 h was ~2 times that of the sample exposed to CH<sub>4</sub> for 10 h in terms of mass concentration calculated using the Wagner method [20]. Thus, the results from XPS analysis are consistent with the TPO results.

#### 3.2. Effect of H<sub>2</sub>S

The introduction of H<sub>2</sub>S may affect the reaction mechanism for carbon deposition. Fig. 5 compares the TPO profiles of the LSBT powders after exposure to CH<sub>4</sub> and 0.5% H<sub>2</sub>S–CH<sub>4</sub> at 1123 K for 24 h. The carbon accumulated in the presence of H<sub>2</sub>S was more

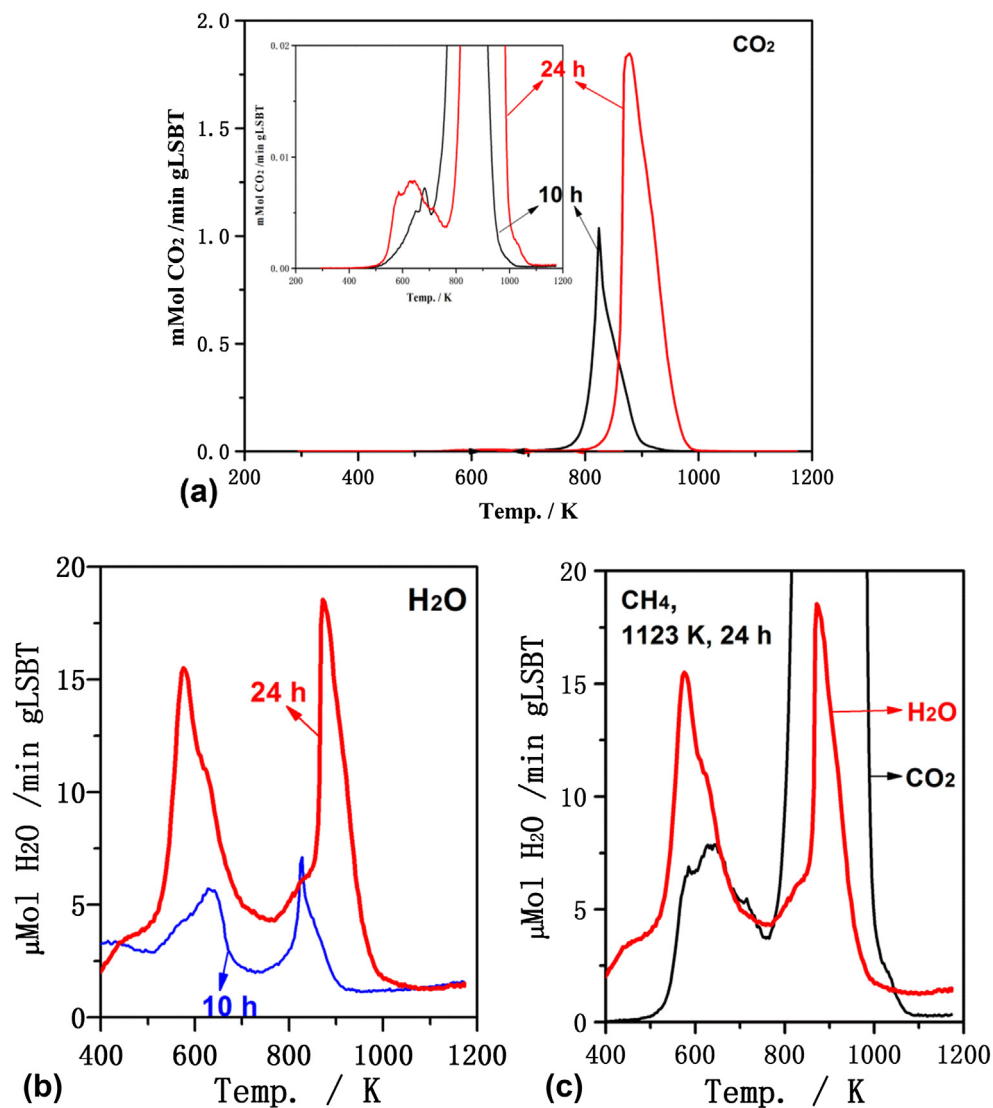


**Fig. 2.** TPO profiles of LSBT powders exposed to CH<sub>4</sub> for 10 h or 24 h at 1123 K: (a) CO<sub>2</sub> production, (b) H<sub>2</sub>O production. (c) CO<sub>2</sub> and H<sub>2</sub>O TPO profiles of LSBT powders exposed to CH<sub>4</sub> for 24 h at 1123 K.

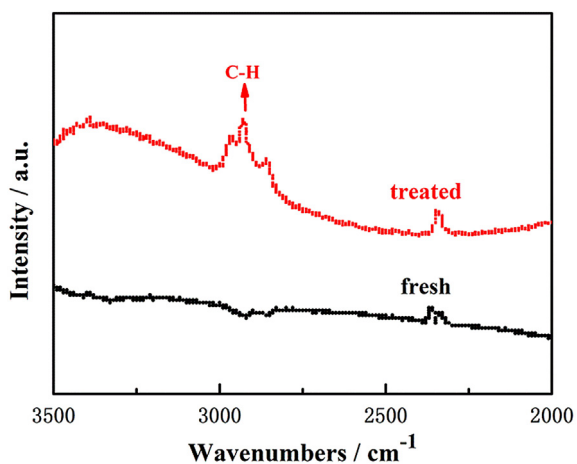


**Fig. 3.** FTIR spectra of the fresh LSBT and the LSBT after treated in CH<sub>4</sub>.

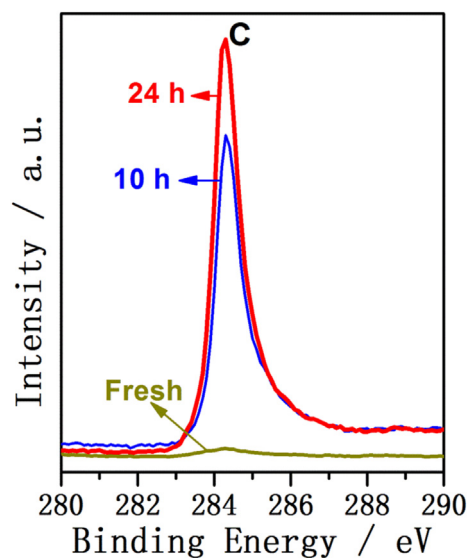


**Fig. 4.** XPS spectra of LSBT powders exposed to CH<sub>4</sub> for 10 h or 24 h at 1123 K.

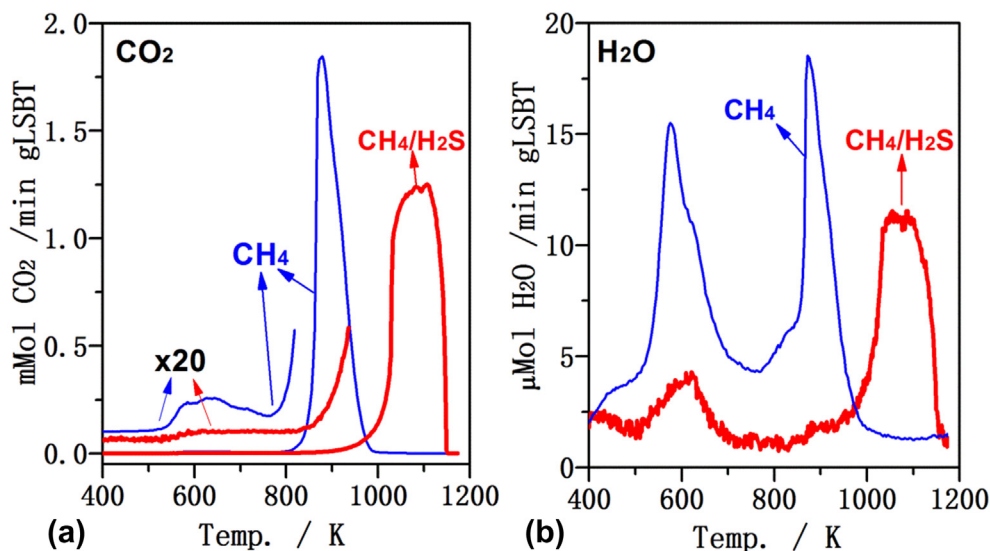


Fig. 5. TPO profiles of LSBT powders exposed to CH<sub>4</sub> or CH<sub>4</sub>/H<sub>2</sub>S for 24 h at 1123 K: (a) CO<sub>2</sub> production and (b) H<sub>2</sub>O production.

stable. That is, for the sample exposed to CH<sub>4</sub>, the high temperature CO<sub>2</sub> peak in the TPO profile extended from 800 to 1050 K, while the high temperature CO<sub>2</sub> peak for the sample exposed to 0.5% H<sub>2</sub>S–CH<sub>4</sub> extended from 900 K to 1150 K. The amount of carbon accumulated on the sample in H<sub>2</sub>S-containing CH<sub>4</sub> was 33% more than that of the sample exposed to pure CH<sub>4</sub> (Table 2).

When the perovskite materials were exposed to H<sub>2</sub>S-containing reducing conditions, sulfur may adsorb onto oxygen deficient surface sites due to the lower oxidation state and oxygen non-stoichiometry of the oxide material [21,22]. This phenomenon can promote carbon accumulation because the adsorbed S blocks the lattice oxygen from oxidizing the deposited carbon species, leading to a higher rate of growth of the graphitic layers. Grgicak demonstrated that adsorbed sulfur provided nucleation points for carbon growth on Co/YSZ anode in the initial stage [2].

To further understand the interaction between CH<sub>4</sub> and H<sub>2</sub>S, surface analysis of the spent powders was done. Fig. 6a shows the full range XPS binding energy spectra of both samples. The binding energies of all component elements remained almost unchanged between the samples, indicating that the LSBT anode catalyst was stable in both environments of methane with and without 0.5% H<sub>2</sub>S. The peak intensities of all component elements, except carbon, however, decreased when H<sub>2</sub>S was introduced, possibly because of an increased amount of carbon on the surface (Fig. 6b). The expanded region in the range of 160–172 eV corresponding to sulfur species is shown in Fig. 6c. As expected, there was no sulfur peak for the sample exposed to pure CH<sub>4</sub>. The intensity of sulfur 2p peak of the sample exposed to 0.5% H<sub>2</sub>S–CH<sub>4</sub> was relatively weak, which would be inevitably affected by the environment noise, showing that the LSBT is a good sulfur tolerant anode catalyst. Nevertheless, the peaks could correspond to elemental sulfur (S, 163.7 eV) or carbon disulfide (CS<sub>2</sub>, 163.7 eV) [22].

Table 2

Amount of CO<sub>2</sub>, CO and H<sub>2</sub>O produced during TPO tests of LSBT powders exposed to various gas mixtures for 24 h at 1123 K.

Feed	Sample mass (g)	CO <sub>2</sub> (mol)	CO (mol)	H <sub>2</sub> O (mol)	Total carbon (mol C g <sup>-1</sup> )
CH <sub>4</sub>	0.1680	2.03E-3	1.9E-4	7.74E-5	1.32E-2
CH <sub>4</sub> /H <sub>2</sub> S	0.3547	5.15E-3	1.09E-3	9.96E-5	1.76E-2
CH <sub>4</sub> +H <sub>2</sub> O	0.1680	1.26E-4	1.7E-5	4.71E-5	0.85E-3
CH <sub>4</sub> /H <sub>2</sub> S + H <sub>2</sub> O	0.1680	1.98E-3	6.88E-4	7.23E-5	1.59E-2

The mechanism of methane oxidation in an H<sub>2</sub>S-containing environment has been previously studied [4,23]. The presence of H<sub>2</sub>S strongly promoted methane oxidation due to the interaction and the synergistic effect between CH<sub>4</sub> and H<sub>2</sub>S. Furthermore, H<sub>2</sub>S may modify the active sites of the anode catalyst and, as such, change the reaction path resulting in improved oxidation [24,25]. Both TPO and XPS analysis indicated that the introduction of H<sub>2</sub>S to the system resulted in increased carbon accumulation (Table 2, Fig. 6b).

H<sub>2</sub>S can decompose into hydrogen and elemental sulfur through the following reactions:



$$\Delta G_{1123\text{ K}}^0 = 184.1 \text{ kJ mol}^{-1}$$



$$\Delta G_{1123\text{ K}}^0 = 70.2 \text{ kJ mol}^{-1}$$

These reactions are endothermic and not spontaneous until temperatures above 1773 K [26], and, thus, not relevant for conditions in this study. With 0.5% H<sub>2</sub>S in the dry CH<sub>4</sub> fuel, the formation of carbon can proceed via an additional pathway than methane dissociation (reaction (1)). Previous work in our group [4] has identified the presence of 200 ppm CS<sub>2</sub> in the anode exhaust gas of the La<sub>0.4</sub>Sr<sub>0.6</sub>TiO<sub>3</sub>/YSZ-based cell exposed to 0.5% H<sub>2</sub>S–CH<sub>4</sub> at OCV after 24 h by analysis using mass spectrometry. The formation of CS<sub>2</sub> can occur as follows:



$$\Delta G_{1123\text{ K}}^0 = 19.5 \text{ kJ mol}^{-1}$$

The reaction of CH<sub>4</sub> reforming with H<sub>2</sub>S (reaction (4)) occurs slowly because the free energy of the reaction ( $\Delta G_{1123\text{ K}}^0$ ) is positive,

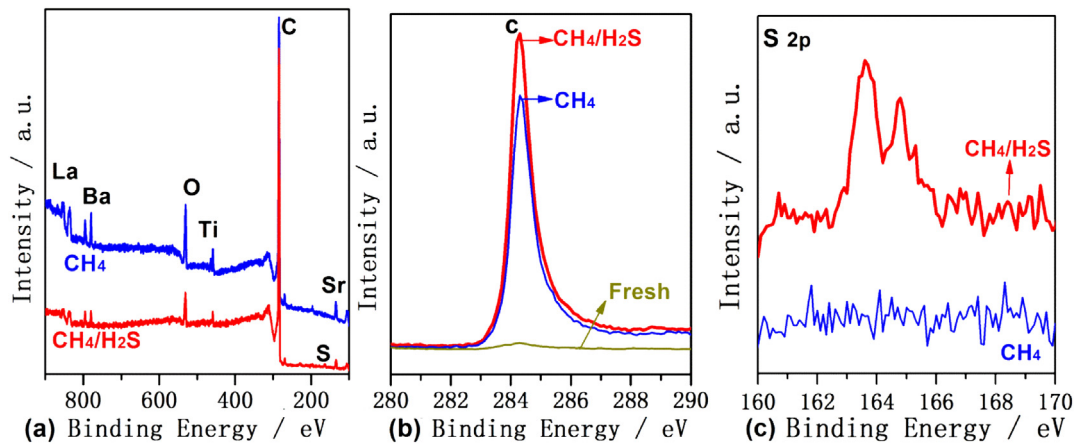


Fig. 6. XPS spectra of LSBT powders exposed to CH<sub>4</sub> or CH<sub>4</sub>/H<sub>2</sub>S for 24 h at 1123 K in (a) full range, (b) C 1s and (c) S 2p binding energy region.

but if formed, CS<sub>2</sub> could undergo dissociation or react with CH<sub>4</sub> as follows:



$$\Delta G_{1123\text{ K}}^{\circ} = 18.1 \text{ kJ mol}^{-1}$$



$$\Delta G_{1123\text{ K}}^{\circ} = -84.7 \text{ kJ mol}^{-1}$$

The Gibbs free energies of the reactions at 1123 K,  $\Delta G_{1123\text{ K}}^{\circ}$ , were obtained from calculations using HSC 5.1 Chemistry software. While these data are just for equilibrium conditions, they can still be used for a fast screening of the possible reactions as well as the equilibrium composition under the SOFC operating conditions.

To evaluate the nature of the carbon accumulated under operating conditions of a SOFC, full cells were prepared and tested under potentiodynamic mode and at constant current densities of 40 mA cm<sup>-2</sup> and 80 mA cm<sup>-2</sup> in 0.5% H<sub>2</sub>S–CH<sub>4</sub> for 24 h at different temperatures. Fig. 7a shows the detailed *I*–*V* and *I*–*P* curves of LSBT/YSZ cells in 0.5% H<sub>2</sub>S–CH<sub>4</sub> at 1073 K and 1123 K, respectively. As expected, the peak power density improved as the temperature increased. Fig. 7b shows the corresponding electrochemical impedance spectra of the cells tested at different temperatures under OCV conditions. Obviously, both the ohmic and polarization resistances reduced with the increasing temperatures, which correspond to the *I*–*P* results shown in Fig. 7a. After treatment, TPO analysis was carried out to determine the amount and types of accumulated carbon as shown in Fig. 8. There was a substantial difference between the TPO profiles for the cells treated under OCV conditions and discharging conditions. In particular, the amount of carbon accumulated under discharging was ~100 times less than that under OCV conditions (Table 3). As the current density increased from 40 mA cm<sup>-2</sup> to 80 mA cm<sup>-2</sup>, the amount of accumulated carbon decreased, but the type of carbon did not significantly change with CO<sub>2</sub> evolution remaining at temperatures between 450 K and 920 K. In contrast, CO<sub>2</sub> evolution occurred at higher temperatures ranging from 900 K to 1150 K when the cell was operated at OCV.

There are several possible reasons for the decrease in carbon deposition under discharging conditions. Increasing the current density leads to an increase in oxygen flux through the electrolyte, which may have oxidized and removed carbon nuclei, formed at the initial stage of deposition, near the TPB [27]. With

increased carbon removal, cell stability improved (i.e., a smaller decrease in voltage over the test) at the higher current density. During the discharging process, the polarization resistance of the cell was also found to decrease as the current density was increased. Bruce and McIntosh [28] demonstrated that the decrease in anode polarization resistance with increasing current density for SOFC directly utilizing hydrocarbons was due to the

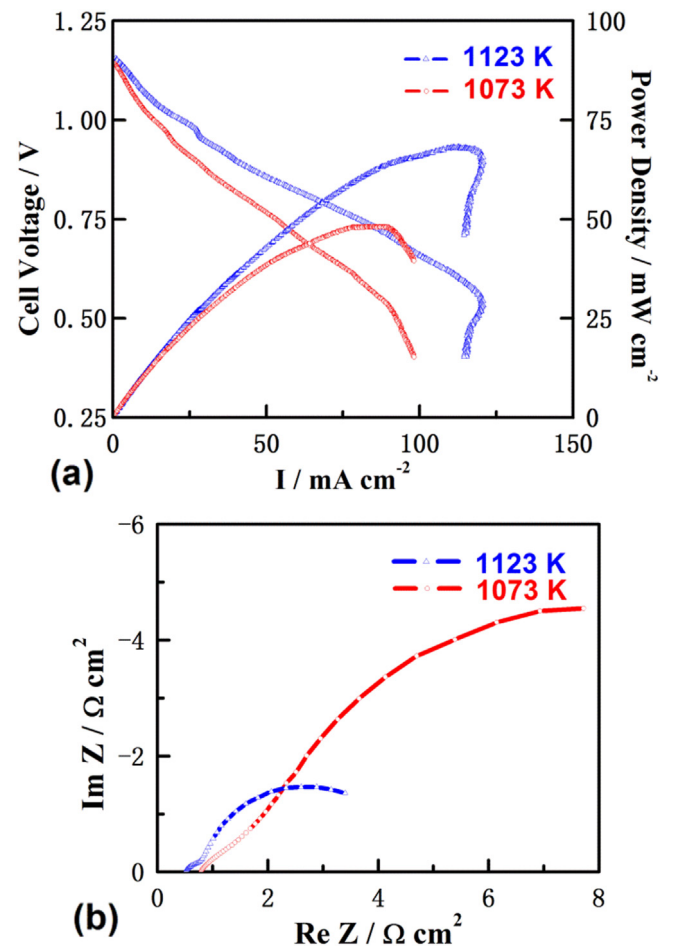


Fig. 7. (a) Current density–voltage and power density curves of LSBT/YSZ cell in 0.5% H<sub>2</sub>S–CH<sub>4</sub> at different temperatures, (b) corresponding impedance spectra of the cell measured under OCV condition.

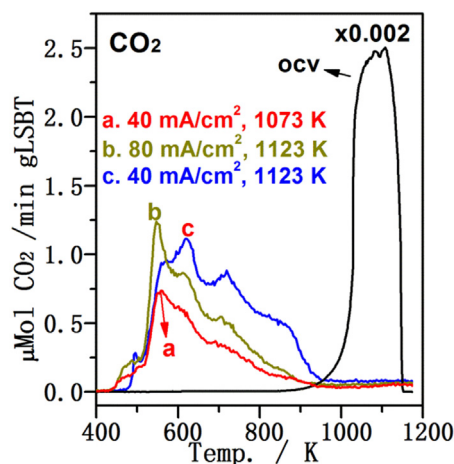


Fig. 8. CO<sub>2</sub> production during TPO tests of the LSBT anode catalysts exposed to 0.5% H<sub>2</sub>S–CH<sub>4</sub> for 24 h at different current densities and temperatures.

Table 3

The amount of CO<sub>2</sub>, CO and H<sub>2</sub>O produced during TPO tests of LSBT anode catalysts exposed to 0.5% H<sub>2</sub>S–CH<sub>4</sub> under various conditions for 24 h.

Condition	Sample mass (g)	CO <sub>2</sub> (mol)	CO (mol)	H <sub>2</sub> O (mol)	Total carbon (mol C g <sup>-1</sup> )
OCV, 1123 K	0.3547	5.15E-3	1.09E-3	9.96E-5	1.76E-2
40 mA cm <sup>-2</sup> , 1073 K	0.1674	1.55E-5	6.21E-6	2.73E-5	1.30E-4
40 mA cm <sup>-2</sup> , 1123 K	0.2047	3.13E-5	1.74E-6	4.66E-5	2.38E-4
80 mA cm <sup>-2</sup> , 1123 K	0.2020	3.53E-5	6.96E-6	3.57E-5	2.08E-4

increased oxygen stoichiometry in the lattice of the perovskite material (ABO<sub>3-δ</sub>) with a corresponding increase in the electro-catalytic oxidation.

The influence of reaction temperature on carbon deposition at 40 mA cm<sup>-2</sup> in 0.5% H<sub>2</sub>S–CH<sub>4</sub> for 24 h was also examined, as shown in Fig. 8 and Table 3. Consistent with other published results [11,27,29,30], the amount and the rate of carbon accumulated increased with operating temperature. In our tests, as the loaded external current density was fixed, the number of oxygen ions migrating through the YSZ electrolyte was the same for both cells.

Thus, the higher amount of carbon accumulated on the anode was attributed to a much faster rate for the fuel cracking reactions at the higher temperature.

### 3.3. Effect of H<sub>2</sub>O

The presence of steam in the feed can inhibit carbon deposition [27] but may also interact with H<sub>2</sub>S and so the combination of these additives to the CH<sub>4</sub> feed was examined. The LSBT powders were exposed to dry CH<sub>4</sub> and CH<sub>4</sub> with 3% water vapor at 1123 K for 24 h. After cooling down to room temperature in flowing 10% H<sub>2</sub>–N<sub>2</sub>, TPO measurements were performed to evaluate the accumulated carbon in both samples. The resulting TPO curves are shown in Fig. 9 and the amount of deposited carbon is shown in Table 2. The amount of carbon formed in humidified methane was approximately 1/16 of that formed in dry methane.

Fig. 10 shows the XPS spectra of the LSBT powders before and after exposure to humidified and dry methane for 24 h at 1123 K. Carbon accumulated even when the CH<sub>4</sub> feed contained 3% water vapor. The amount of carbon, however, was much less compared to that formed in dry methane, consistent with the TPO analysis. In the presence of steam, carbon can be gasified (reaction (7)), and methane reformed (reaction (8)), which will both contribute to decreasing carbon accumulation. As less carbon accumulated, there was less chance for graphite to form and so the carbon could be removed at lower temperatures in the TPO analysis (Fig. 9a) and this carbon contained more hydrogen.



$$\Delta G_{1123\text{ K}}^0 = -25.2 \text{ kJ mol}^{-1}$$



$$\Delta G_{1123\text{ K}}^0 = -57.8 \text{ kJ mol}^{-1}$$

When steam was added to the 0.5% H<sub>2</sub>S–CH<sub>4</sub> feed, the accumulated carbon on the LSBT powders changed somewhat. That is, the high temperature CO<sub>2</sub> peak in the TPO profile decreased

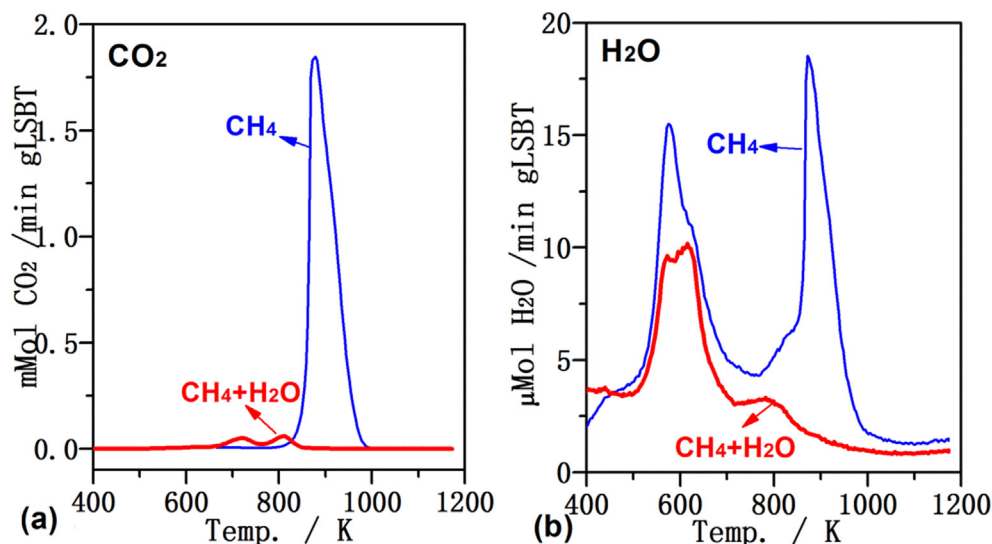


Fig. 9. TPO profiles of LSBT powders exposed to CH<sub>4</sub> or CH<sub>4</sub> + H<sub>2</sub>O for 24 h at 1123 K: (a) CO<sub>2</sub> production and (b) H<sub>2</sub>O production.

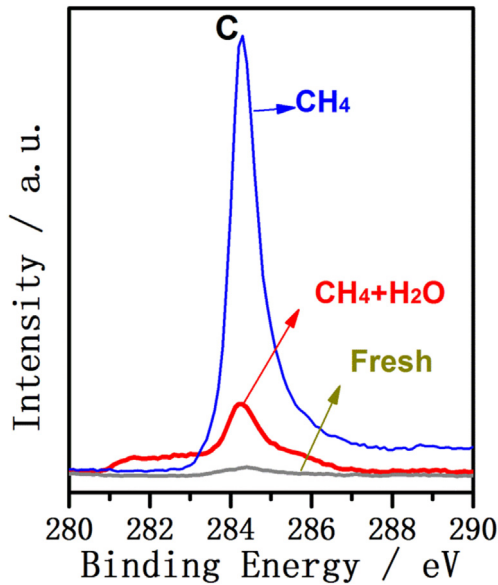


Fig. 10. XPS spectra of LSBT powders exposed to CH<sub>4</sub> or CH<sub>4</sub> + H<sub>2</sub>O for 24 h at 1123 K.

from 900–1150 K to 900–1100 K (Fig. 11a). According to the XPS (Fig. 12) and TPO (Table 2) analysis results, there was no significant decrease in the amount of deposited carbon when steam was added to the feed with a C:H ratio of 1.9, compared to a C:H ratio of 2.5 for the LSBT sample exposed to dry 0.5% H<sub>2</sub>S-containing methane feed. It is possible that carbon nucleation due to the adsorbed S increases the rate of graphitic film formation (fast breakdown of CH<sub>x</sub> groups), making it difficult for the co-fed H<sub>2</sub>O to have an effect by gasifying the CH<sub>x</sub> groups. Thus, steam was ineffective at suppressing carbon accumulation in the presence of H<sub>2</sub>S. Additional reactions are possible for the H<sub>2</sub>S-containing CH<sub>4</sub> system, which may interfere with the steam gasification of the deposited carbon [4]. Steam can react with CS<sub>2</sub> formed through reaction (4) to form either COS (reaction (9)) or CO<sub>2</sub> (reaction (10)).



$$\Delta G_{1123\text{ K}}^0 = -48.2 \text{ kJ mol}^{-1}$$



$$\Delta G_{1123\text{ K}}^0 = -76.3 \text{ kJ mol}^{-1}$$

Carbon deposition may be suppressed indirectly by CO<sub>2</sub> reforming of CH<sub>4</sub> (reaction (11)), and directly by reacting with deposited carbon (reaction (12)).



$$\Delta G_{1123\text{ K}}^0 = -58.8 \text{ kJ mol}^{-1}$$



$$\Delta G_{1123\text{ K}}^0 = -26.2 \text{ kJ mol}^{-1}$$

#### 4. Conclusions

In this work, we have examined the effects of H<sub>2</sub>S and H<sub>2</sub>O in the methane feed on carbon deposition over LSBT/YSZ powders and anodes at different operating conditions. The amount and stability of the deposited carbon increased with increasing exposure time and increasing operating temperatures. When electrical current was drawn from the cell, the amount of the carbon deposition was about 100 times less than that under OCV conditions, and the accumulated carbon was more reactive. Further increasing the current density from 40 mA cm<sup>-2</sup> to 80 mA cm<sup>-2</sup>, decreased the amount of carbon accumulated but did not significantly change the type of carbon. Introduction of 0.5% H<sub>2</sub>S to the methane feed resulted in a lower reactivity of the accumulated carbon toward oxidation. Although the addition of steam to the methane feed decreased carbon accumulation, in the presence of 0.5% H<sub>2</sub>S, carbon accumulation could not be fully suppressed by the steam. Nevertheless, LSBT anodes may be suitable for SOFCs operated on natural gas.

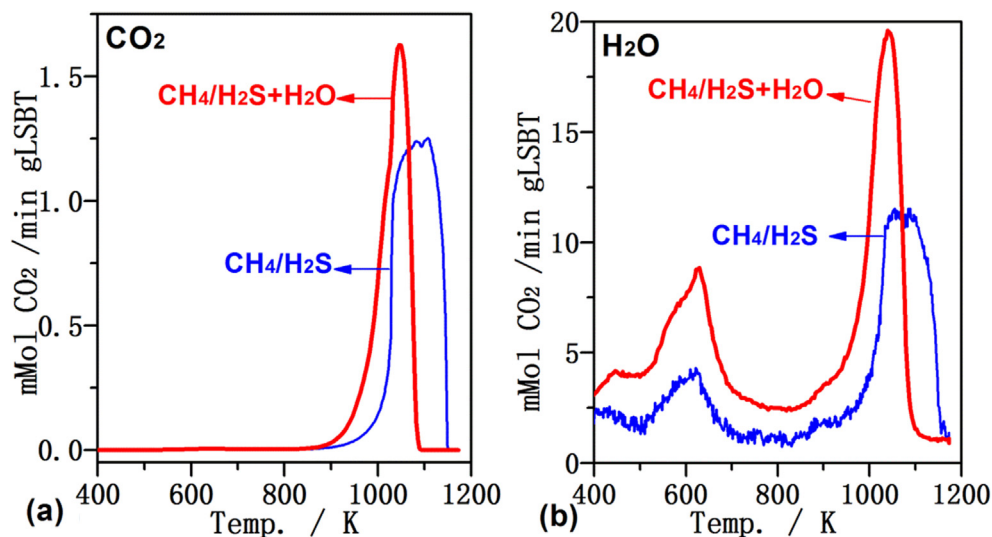
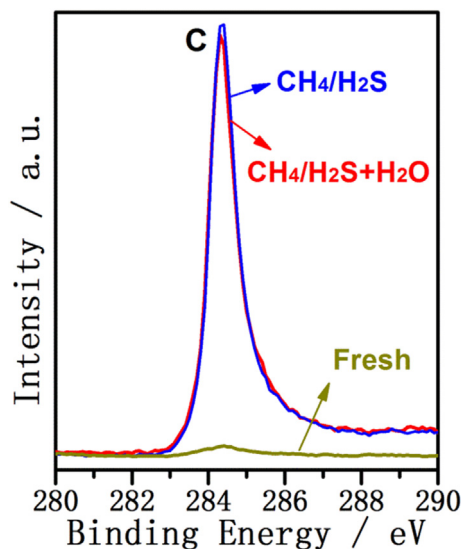


Fig. 11. TPO profiles of LSBT powders exposed to CH<sub>4</sub>/H<sub>2</sub>S or CH<sub>4</sub>/H<sub>2</sub>S + H<sub>2</sub>O for 24 h at 1123 K: (a) CO<sub>2</sub> production and (b) H<sub>2</sub>O production.



**Fig. 12.** XPS spectra of LSBT powders exposed to  $\text{CH}_4/\text{H}_2\text{S}$  or  $\text{CH}_4/\text{H}_2\text{S} + \text{H}_2\text{O}$  for 24 h at 1123 K.

### Acknowledgments

This research was supported through funding to the Solid Oxide Fuel Cell Canada Strategic Research Network from NSERC. The authors gratefully acknowledge financial support from China Scholarship Council.

### References

- [1] E.P. Murray, T. Tsai, S.A. Barnett, *Nature* 400 (1999) 649–651.
- [2] C.M. Grgicak, R.G. Green, J.B. Giorgi, *J. Power Sources* 179 (2008) 317–328.

- [3] A. Lussier, S. Sofie, J. Dvorak, Y.U. Idzerda, *Int. J. Hydrogen Energy* 33 (2008) 3945–3951.
- [4] A.L. Vincent, J.L. Luo, K.T. Chuang, A.R. Sanger, *Appl. Catal., B: Environ.* 106 (2011) 114–122.
- [5] A. Atkinson, S. Barnett, R.J. Gorte, J.T.S. Irvine, A.J. Mcevoy, M. Mogensen, S.C. Singhal, J.M. Vohs, *Nat. Mater.* 3 (2004) 17–27.
- [6] X.F. Sun, S.R. Wang, Z.R. Wang, X.F. Ye, T.L. Wen, F.Q. Huang, *J. Power Sources* 183 (2008) 114–117.
- [7] A. Vincent, J.L. Luo, K.T. Chuang, A.R. Sanger, *J. Power Sources* 195 (2010) 769–774.
- [8] M.D. Gross, J.M. Vohs, R.J. Gorte, *J. Mater. Chem.* 17 (2007) 3071–3077.
- [9] J.N. Armor, D.J. Martenak, *Appl. Catal., A: Gen.* 206 (2001) 231–236.
- [10] H. Kan, H. Lee, *Appl. Catal., B: Environ.* 97 (2010) 108–114.
- [11] M.A. Bucchieri, A. Singh, J.M. Hill, *J. Power Sources* 196 (2011) 968–976.
- [12] M. Mogensen, K. Kammer, *Annu. Rev. Mater. Res.* 33 (2003) 321–331.
- [13] A.L. Vincent, A.R. Hanifi, J.L. Luo, K.T. Chuang, A.R. Sanger, T.H. Etsell, P. Sarkar, *J. Power Sources* 215 (2012) 301–306.
- [14] T. Kim, G. Liu, M. Boaro, S.I. Lee, J.M. Vohs, R.J. Gorte, O.H. Al-Madhi, B.O. Dabbousi, *J. Power Sources* 155 (2006) 231–238.
- [15] V. Alzate-Resertero, J.M. Hill, *Appl. Catal., A: Gen.* 342 (2008) 49–55.
- [16] M.B. Pomfret, J. Marda, G.S. Jackson, B.W. Eichhorn, A.M. Dean, R.A. Walker, *J. Phys. Chem. C* 112 (2008) 5232–5240.
- [17] T. Jiang, K. Xu, *Carbon* 33 (1995) 1663–1671.
- [18] S. Osswald, G. Yushin, V. Mochalin, S.O. Kucheyev, Y. Gogotsi, *J. Am. Chem. Soc.* 128 (2006) 11635–11642.
- [19] S.W. Lee, B.S. Kim, S. Chen, Y.S. Horn, P.T. Hammond, *J. Am. Chem. Soc.* 131 (2009) 671–679.
- [20] C.D. Wagner, *J. Vac. Sci. Technol., A* 15 (1978) 518.
- [21] M.Y. Gong, X.B. Liu, J. Tremblay, C. Johnson, *J. Power Sources* 168 (2007) 289–298.
- [22] B.J. Lindberg, K. Hamrin, G. Johansson, U. Gelius, A. Fahlman, C. Nordling, K. Siegbahn, *Phys. Scr.* 1 (1970) 286.
- [23] Z. Cheng, S.W. Zha, L. Aguilar, D. Wang, J. Winnick, M.L. Liu, *Electrochem. Solid-state Lett.* 9 (2006) A31–A33.
- [24] M. Roushanafshar, J.L. Luo, A.L. Vincent, K.T. Chuang, A.R. Sanger, *Int. J. Hydrogen Energy* 37 (2012) 7762–7770.
- [25] M. Roushanafshar, J.L. Luo, K.T. Chuang, A.R. Sanger, *ECS Trans.* 35 (2011) 2799–2804.
- [26] C.P. Huang, A.T. Raissi, *J. Power Sources* 175 (2008) 464–472.
- [27] Z.R. Xu, X.Z. Fu, J.L. Luo, K.T. Chuang, *J. Electrochem. Soc.* 157 (2010) B1556–B1560.
- [28] M.K. Bruce, M.v.d. Bossche, S. McIntosh, *J. Electrochem. Soc.* 155 (2008) B1202–B1209.
- [29] H.P. He, J.M. Hill, *Appl. Catal., A: Gen.* 317 (2007) 284–292.
- [30] H.P. He, J.M. Vohs, R.J. Gorte, *J. Power Sources* 144 (2005) 135–140.